

Pressure-induced and Composition-induced Structural Quantum Phase Transition in the Cubic Superconductor (Sr/Ca)₃Ir₄Sn₁₃

Lina E. Klintberg,¹ Swee K. Goh,^{1,*} Patricia L. Alireza,¹ Paul J. Saines,² David A. Tompsett,^{1,†} Peter W. Logg,¹ Jinhu Yang,^{3,4} Bin Chen,^{3,4} Kazuyoshi Yoshimura,⁴ and F. Malte Grosche¹

¹*Cavendish Laboratory, University of Cambridge,
J.J. Thomson Avenue, Cambridge CB3 0HE, United Kingdom*

²*Department of Materials Science and Metallurgy, University of Cambridge,
Pembroke Street, Cambridge CB2 3QZ, United Kingdom*

³*Department of Physics, Graduate School of Science,
Hangzhou Normal University, Hangzhou 310036, China*

⁴*Department of Chemistry, Graduate School of Science, Kyoto University, Kyoto 606-8502, Japan*
(Dated: October 08, 2012)

We show that the quasi-skutterudite superconductor Sr₃Ir₄Sn₁₃ undergoes a structural transition from a simple cubic parent structure, the *I*-phase, to a superlattice variant, the *I'*-phase, which has a lattice parameter twice that of the high temperature phase. We argue that the superlattice distortion is associated with a charge density wave transition of the conduction electron system and demonstrate that the superlattice transition temperature T^* can be suppressed to zero by combining chemical and physical pressure. This enables the first comprehensive investigation of a superlattice quantum phase transition and its interplay with superconductivity in a cubic charge density wave system.

Structural self-organisation is a central theme in condensed matter physics. Often, the symmetry of a given parent structure is lowered by subtle structural variations which decrease the electronic degeneracy and thereby the total energy. Examples include Jahn-Teller [1] and Peierls distortions [2] and, more generally, modulated lattice distortions, or superlattices. A very diverse family of materials can be explored within the general R₃T₄X₁₃ stoichiometry, where R is an earth alkaline or rare-earth element, T is a transition metal and X is a group-IV element. Among these are the superconducting and magnetic stannides [3, 4], Ce-based Kondo lattice systems [5], and thermoelectrics [6]. Many members of this family adopt a variant structure, the *I'*-phase, derived from the simple cubic parent structure (*I*-phase, $Pm\bar{3}n$). Empirically, compounds with divalent or tetravalent cations R occur in the *I*-phase, whereas compounds with trivalent cations form in the *I'*-phase. Detailed diffraction studies [7–9] disagree about the precise *I'*-phase structure, but consistently interpret it as a deformation of the X₁₂ cages, which can be viewed as a superlattice distortion of the *I*-phase with twice the original lattice constant.

A recent reexamination [10] of Ca₃Ir₄Sn₁₃, which superconducts below $T_c = 7$ K, revealed distinct anomalies in the electrical resistivity and magnetic susceptibility at $T^* \simeq 33$ K. In the isoelectronic sister-compound Sr₃Ir₄Sn₁₃, the equivalent anomaly occurs at $T^* \simeq 147$ K and superconductivity sets in at $T_c = 5$ K. Intermediate compositions (Ca_{*x*}Sr_{1-*x*})₃Ir₄Sn₁₃ form readily. This invites studies which exploit the negative chemical pressure from partial substitution of Ca by Sr, together with positive physical pressure from a hydrostatic pressure cell. In this Letter, we report a detailed investigation of the nature of the transition at T^* by x-ray diffraction (XRD), and we examine the dependence of T^* and of the superconducting and normal state properties on physical and chemical pressure. We find that (i) the T^* anomaly is produced by a second order superlattice

transition into the *I'*-phase, (ii) T^* is suppressed with increasing pressure and extrapolates to zero temperature at $p_c \simeq 18$ kbar in Ca₃Ir₄Sn₁₃, and (iii) T_c peaks near p_c , and the electrical resistivity adopts a linear temperature dependence over a wide range of temperature and magnetic field close to this critical pressure.

The (Ca_{*x*}Sr_{1-*x*})₃Ir₄Sn₁₃ single crystals were grown by a flux method [4]. Four-wire AC resistivity measurements were performed in a piston-cylinder cell, using a Physical Property Measurement System (Quantum Design) to control temperature, T . Two Moissanite anvil cells were prepared for AC susceptibility measurements with a conventional mutual inductance method, in which a 10-turn microcoil [11–13] is placed inside the gasket hole (thickness: 150 μm , diameter: 400 μm) as the pickup coil. Glycerin was used as the pressure medium for the piston-cylinder cell and for one of the anvil cells, and 4:1 methanol-ethanol mixture was used for the other anvil cell. Ruby fluorescence spectroscopy and the T_c of lead were used to determine the pressure in the anvil and piston-cylinder cell respectively. Single crystal XRD measurements were performed using an Oxford Diffraction Gemini E Ultra utilising MoK α radiation at 100 to 295 K. The structures were solved using direct methods and refined using Shelx-97 [14] via the WinGX interface [15]. The electronic structure was calculated using the Local Density Approximation (LDA) and the Generalized Gradient Approximation (GGA) [16] with Wien2k [17]. $Rk_{max} = 7$ and 40,000 k -points were used in a non-spin polarized calculation. The position of the 24*k* Sn site (0, y , z), the only free internal coordinate, was optimised numerically, resulting in (0, $y = 0.3045$, $z = 0.1516$) and (0, $y = 0.3027$, $z = 0.1522$) for Ca- and Sr₃Ir₄Sn₁₃ respectively.

Room temperature single crystal XRD confirms that Sr₃Ir₄Sn₁₃ forms in the *I*-phase structure ($Pm\bar{3}n$, lattice parameter $a = 9.7968(3)$ Å at 295 K, inset of Fig. 1a). On cooling, distinct signatures of a phase transition at

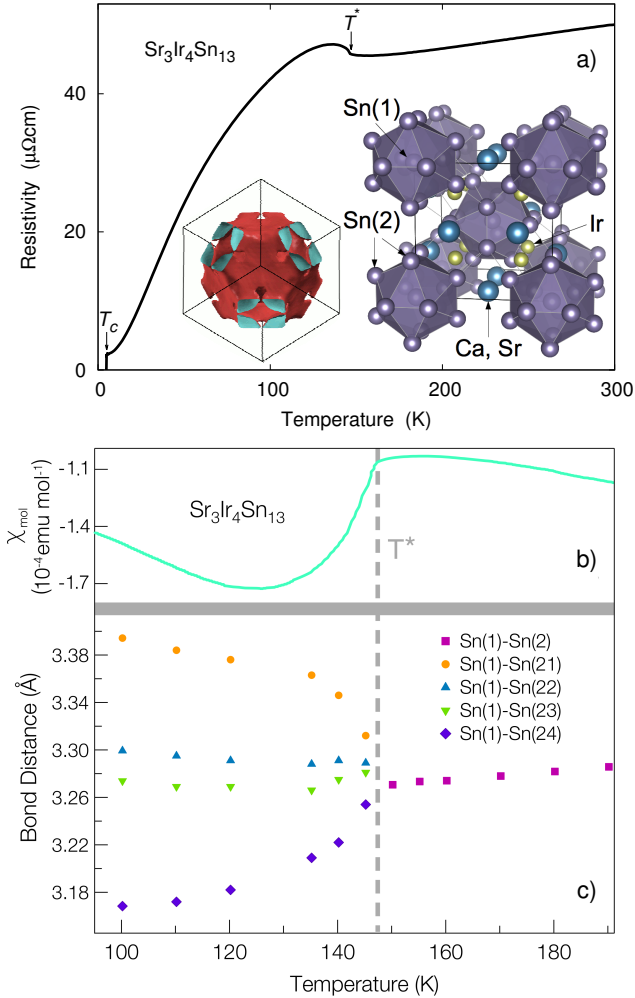


FIG. 1. Key properties of $\text{Sr}_3\text{Ir}_4\text{Sn}_{13}$ at ambient pressure. The main panels show the temperature dependence of (a) the electrical resistivity, (b) the magnetic susceptibility, and (c) interatomic bond-lengths. The right inset to panel (a) illustrates the crystal structure of $\text{Sr}_3\text{Ir}_4\text{Sn}_{13}$, featuring Sn(2) 12-cages (icosahedra), which each contain a central Sn(1) atom. The bond-length between the central Sn atom and the cage atoms the I -phase, splits into four distinct lengths in the I' -phase below $T^* \simeq 147$ K. The symbol sizes represent the measurement accuracy. The left inset to panel (a) shows one of the larger Fermi surface sheets (band 329) computed in the I -phase of $\text{Sr}_3\text{Ir}_4\text{Sn}_{13}$.

$T^* = 147$ K are observed in the temperature dependence of the electrical resistivity ρ and of the magnetic susceptibility χ of $\text{Sr}_3\text{Ir}_4\text{Sn}_{13}$, in addition to a superconducting transition at $T_c = 5$ K (Fig. 1). Below T^* our single crystal XRD data are inconsistent with the I -phase. They must instead be indexed [18] to the I' -phase, a body(I)-centered cubic structure with a lattice parameter twice that of the high temperature phase ($I43d$, $a = 19.5947(3)$ Å at 100 K, $R1$, $wR2$ and χ^2 of 4.4 %, 13.9 % and 1.1 %, respectively). In the I -phase, the bond distances in the Sn(1)Sn(2)₁₂ icosahedra and in the IrSn(2)₆ trigonal prisms which connect them are identical. In the I' -phase, however, a distortion of the Sn(2) icosahedra gives rise to four groups, Sn(1)-Sn(21-24), each group composed of three bonds with identi-

TABLE I. Interplay between lattice and electronic structure in $\text{Sr}_3\text{Ir}_4\text{Sn}_{13}$, investigated by *ab initio* simulation using density functional theory (DFT) with local (LDA) and gradient-corrected (GGA) semi-local functionals. Lattice parameters a and electronic density of states at the Fermi energy $g(E_F)$ have been computed after full structural relaxation in both the I and I' phase. ΔE is the difference in total energy between the two phases. The lower DOS and total energy obtained for the I' -phase agree with the experimental observation that $\text{Sr}_3\text{Ir}_4\text{Sn}_{13}$ adopts the I' structure at low temperature, and the small magnitude of ΔE is consistent with the low transition temperature T^* .

	GGA calculation			LDA calculation		
	a Å	$g(E_F)$ (f.u. eV) ⁻¹	ΔE meV/f.u.	a Å	$g(E_F)$ (f.u. eV) ⁻¹	ΔE meV/f.u.
I	9.937	12.5		9.698	12.5	
I'	2 · 9.941	9.3	-7.1	2 · 9.700	8.5	-3.4

cal bond distances (see Fig. 1c). This distortion occurs in concert with tilting of three-quarters of the trigonal prisms while those whose axis are along the (111) direction remain untilted. Because of the periodic nature of this distortion, it leads to the formation of a superlattice.

Electronic structure calculations give further insight into the nature of this superlattice transition. Our calculations (Table I) suggest that in $\text{Sr}_3\text{Ir}_4\text{Sn}_{13}$ the I' -phase superlattice has a slight energy advantage with respect to the I -phase parent structure. Moreover, the period-doubling associated with the superlattice causes the large Fermi surface sheets computed for the I -phase (e.g. left inset in Fig. 1a) to reconstruct, which gaps out significant sections of the Fermi surface. The calculated reduction in the electronic density of states at the Fermi energy amounts to nearly 30%, or $\simeq 3.5$ eV⁻¹ per formula unit, which translates to a change in the Pauli susceptibility of $\Delta\chi = \mu_0\mu_B^2 g(E_F) \simeq 1.1 \cdot 10^{-4}$ emu/mol. This value is consistent with the observed reduction of the measured susceptibility at T^* (Fig. 1b). The distinct increase of $\rho(T)$ below T^* may also be attributed at least in part to the reduction in $g(E_F)$, along with other factors, such as changes in the effective carrier mass and the scattering rate.

The significant reduction of $g(E_F)$ on entering the I' -phase indicates that electronic states near the Fermi energy play an important role in forming the superlattice, which suggests a charge density wave (CDW) instability of the conduction electron system. In the I -phase, six bands cross the Fermi level. Each sheet of the Fermi surface is three dimensional, but some sheets exhibit low curvature regions with the necessary characteristics for nesting: the flat sections of band 329 (inset of Fig. 1a) are strong candidates. The contribution of this band to the real part of the wavevector-dependent charge susceptibility $\chi(\mathbf{q})$, or Lindhard function, peaks at $\mathbf{q} = (1/2, 1/2, 1/2)$, with a 21% enhancement above that at the Brillouin zone centre [18]. This confirms the visual impression that sections of the Fermi surface nest along the body diagonal and is consistent with the experimentally observed doubling of the lattice parameter in all directions. As in most CDW systems [19], the re-

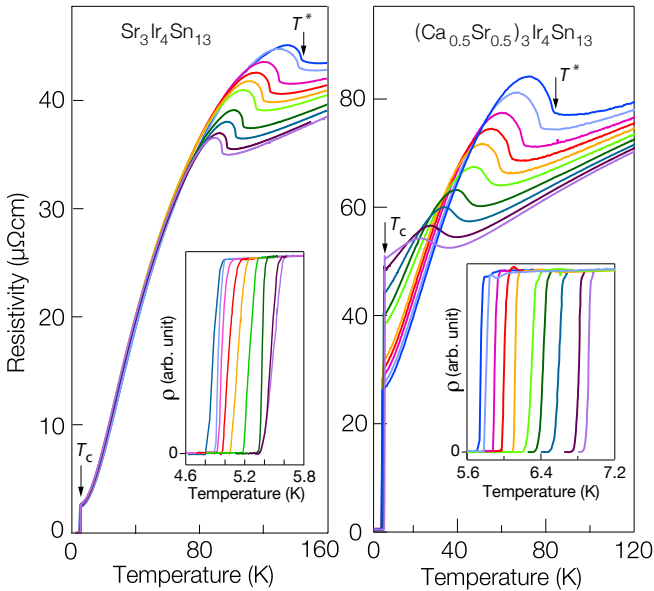


FIG. 2. High pressure resistivity data in $\text{Sr}_3\text{Ir}_4\text{Sn}_{13}$ (left) and in mid-way Ca-substituted $(\text{Sr}_{0.5}\text{Ca}_{0.5})_3\text{Ir}_4\text{Sn}_{13}$, showing both the superlattice and superconducting transitions. The pressures are given by 1.1, 3.8, 8.7, 11.7, 13.7, 17.3, 19.3, 21.8, 23.5, 25.7 kbar in sequential order with the highest T^* at the lowest pressure. The insets show expanded views of the superconducting transitions.

sponse of the conduction electrons in isolation is not singular, but strong electron-phonon interactions can induce an instability at the wavevector selected by the peak in the Lindhard function. Our calculations suggest that the low temperature I' -phase is stabilised by the interplay between a periodic lattice distortion and a CDW in the conduction electron system.

High-pressure measurements of the resistivity, $\rho(T)$, in $\text{Sr}_3\text{Ir}_4\text{Sn}_{13}$ show that T^* decreases rapidly with increasing pressure, p , whereas T_c rises slowly (Fig. 2a). This pattern carries over to partially Ca-substituted samples such as $(\text{Sr}_{0.5}\text{Ca}_{0.5})_3\text{Ir}_4\text{Sn}_{13}$ (Fig. 2b), which due to its smaller unit cell volume can be regarded as a high pressure analogue of $\text{Sr}_3\text{Ir}_4\text{Sn}_{13}$. In the end member of this series, $\text{Ca}_3\text{Ir}_4\text{Sn}_{13}$ (Fig. 3), the resistivity anomaly associated with T^* broadens and T^* decreases further with increasing pressure, extrapolating to 0 K at a critical pressure $p_c \simeq 18$ kbar (see also Fig. 4). This constitutes a structural quantum phase transition or, if the transition remains continuous, a structural quantum critical point. Near p_c , $\rho(T)$ is linear over a wide temperature range, from T_c up to 50 K. Anvil cell AC susceptibility measurements extend the available pressure range and show that T_c peaks near 8.9 K at $\simeq 40$ kbar (inset of Fig. 3).

Analysis of the pressure dependence of T^* and T_c at intermediate substitution values x suggests that the effect of fully substituting Ca with Sr places $\text{Sr}_3\text{Ir}_4\text{Sn}_{13}$ at roughly -52 kbar relative to the physical pressure scale of $\text{Ca}_3\text{Ir}_4\text{Sn}_{13}$. Applying Vegard's law to intermediate composition values allows us to construct a universal temperature-pressure phase diagram for the $(\text{Ca}_x\text{Sr}_{1-x})_3\text{Ir}_4\text{Sn}_{13}$ series (Fig. 4). The observation of

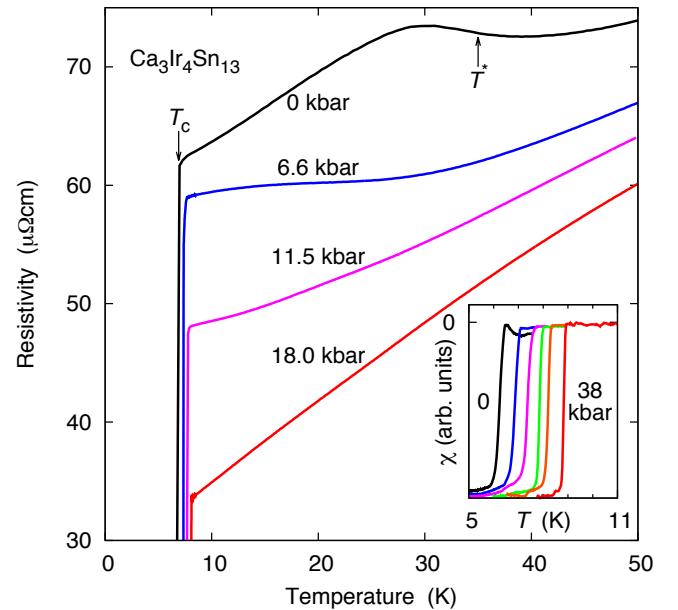


FIG. 3. (Main panel) Temperature dependence of the electrical resistivity in $\text{Ca}_3\text{Ir}_4\text{Sn}_{13}$ at different applied hydrostatic pressures. T^* is defined as the minimum of $d\rho/dT$, which broadens on approaching the critical point. Near the critical pressure $p_c \simeq 18$ kbar, where T^* extrapolates to 0 K, $\rho(T)$ assumes a linear temperature dependence over a large temperature range. (Inset) Superconducting transitions in $\text{Ca}_3\text{Ir}_4\text{Sn}_{13}$ observed in the magnetic susceptibility at, from the left, 0, 7, 57, 48, 28 and 38 kbar. T_c peaks near 8.9 K at about 40 kbar.

a superconducting dome, which peaks close to p_c , and the anomalous quasi-linear $\rho(T)$ are often associated with quantum critical phenomena on the threshold of magnetism [20]. There is, however, no evidence that the low temperature order observed in $(\text{Sr}/\text{Ca})_3\text{Ir}_4\text{Sn}_{13}$ is magnetic. On the contrary, the fact that no magnetic order has been reported in any other I' -phase material without rare-earth constituents, the low absolute magnetic susceptibility values, the absence of clear anisotropy in the susceptibility at T^* , our spin polarised band structure calculations within density functional theory for various hypothetical magnetic states, in which the magnetic moments collapse to zero in all cases, and the strong indications that the superconducting state is conventional and fully gapped [21, 22] all point towards a non-magnetic transition at T^* . Because $g(E_F)$ is strongly reduced in the I' -phase (Table I), conventional BCS theory suggests that the associated T_c is low compared to the value that could be achieved in the I -phase. Conversely, when T^* is suppressed with hydrostatic pressure, and the I -phase survives to low temperatures, $g(E_F)$ increases. This would be expected to raise T_c on approaching p_c , as is indeed observed.

To understand the initial further increase of T_c for $p > p_c$, the decrease of T_c at much higher pressures and the linear temperature dependence of $\rho(T)$ near p_c (Fig. 3) we need to look beyond $g(E_F)$ and examine the evolution of the phonon spectrum. If the superlattice transition remains second order or only weakly first

order, then the associated optical phonon mode should soften at T^* , which itself approaches zero at p_c . This generates a low-lying, weakly dispersive phonon branch at low temperature. We would expect its contribution to the electrical resistivity to become linear in temperature, in analogy with the behaviour of simple metals above the Debye temperature, once the thermal energy $k_B T$ exceeds the maximum phonon energy of this branch. A more detailed argument along the lines presented for Einstein solids [23, 24], notes that the phonon contribution to the electrical resistivity can be written as

$$\Delta\rho_{ph}(T) \propto \sum_{\mathbf{q}} \alpha_{(tr)\mathbf{q}}^2 T (\partial n_{\mathbf{q}}/\partial T)_{\omega_{\mathbf{q}}} . \quad (1)$$

The sum is taken over all phonon wavevectors \mathbf{q} within a suitable cut-off, and $\alpha_{(tr)\mathbf{q}}^2$ is a \mathbf{q} -dependent Fermi surface average of the electron-phonon interaction, which is proportional to the density of states at the Fermi energy, has been weighted appropriately for transport calculations, and depends weakly on \mathbf{q} away from $q = 0$. Moreover, $\omega_{\mathbf{q}}$ denotes the \mathbf{q} -dependent phonon frequency, and $n_{\mathbf{q}} = [\exp(\hbar\omega_{\mathbf{q}}/(k_B T)) - 1]^{-1}$ is the Bose occupation number. When $k_B T$ exceeds the highest $\hbar\omega_{\mathbf{q}}$, this expression reverts to $T \sum \omega_{\mathbf{q}}^{-1}$, giving a T -linear resistivity, which is strongly enhanced for low $\omega_{\mathbf{q}}$. Because the electron-phonon coupling constant λ can be expressed as $\lambda = 2 \sum_{\mathbf{q}} \alpha_{\mathbf{q}}^2 \omega_{\mathbf{q}}^{-1}$ (see, e.g. [25]), where $\alpha_{\mathbf{q}} \simeq \alpha_{(tr)\mathbf{q}}$ for large q , it is seen to be directly connected to the slope of the T -linear resistivity.

The softening of parts of the phonon spectrum can also help explain the shape of the superconducting dome (see, e.g. [26]). In the Eliashberg-McMillan treatment [25] T_c is exponentially sensitive to λ , which in turn is proportional to $g(E_F)$ and to $\sum \omega_{\mathbf{q}}^{-1}$. As T^* is reduced, the removal of Fermi surface reconstruction raises $g(E_F)$, while the softening of parts of the phonon spectrum increases $\sum \omega_{\mathbf{q}}^{-1}$. Both effects tend to increase λ , which, if all other parameters are constant, raises T_c . Beyond these considerations, the precise effect of a soft mode on T_c has to be considered in order to understand the shape of the superconducting dome for pressures above p_c . Whereas T_c depends exponentially on λ , its scale prefactor is set by a weighted average of $\omega_{\mathbf{q}}$. The combined effect of scale and exponent is not necessarily optimised at the point where an optical mode is soft, as this minimises the scale prefactor. We would, instead, expect the peak to occur slightly beyond the critical point in the phase diagram, as found experimentally (Fig. 4). Eventually, the optical mode associated with the superlattice transition stiffens sufficiently so that the detrimental effect this has on λ begins to reduce T_c . Detailed theoretical calculations based on more complete information about the phonon spectrum will be required to arrive at a quantitative understanding of the observed phase diagram.

Investigations into the effect of lattice instabilities on superconductivity have a long history, starting with the structurally related A15 compounds [27, 28]. Examples of enhanced superconductivity near lattice instabilities include $\text{Lu}_5\text{Ir}_4\text{Si}_{10}$ [29], dichalcogenides such as TiSe_2 [30, 31] and TaS_2 [32], intercalated graphite CaC_6 [33],

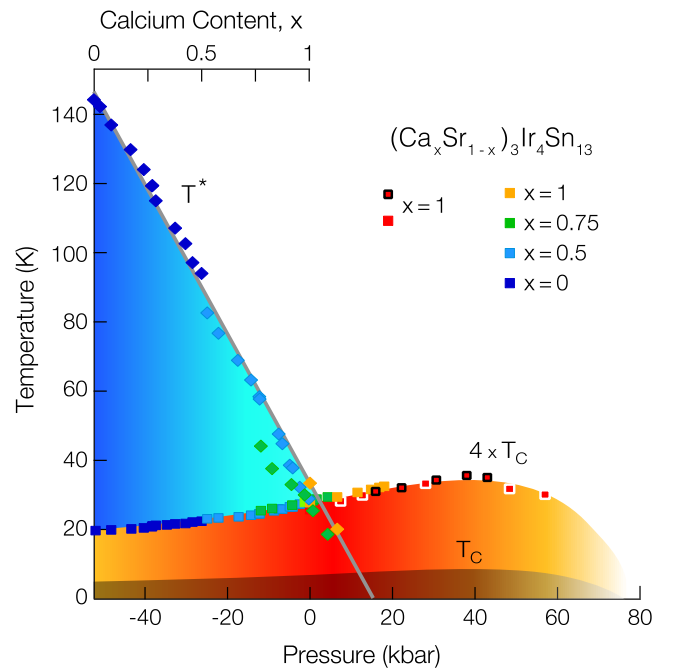


FIG. 4. Universal phase diagram for the $(\text{Ca}_x\text{Sr}_{1-x})_3\text{Ir}_4\text{Sn}_{13}$ system, constructed by placing $x = 0, 0.50$ and 0.75 at $-52, -26$ and -13 kbar, respectively (c.f. top axis). The superlattice transition temperature, T^* , extrapolates to zero temperature at roughly 18 kbar. The red ($x = 1$) symbols denote values derived from AC susceptibility measurements – the white (black) borders represent a pressure medium of glycerin (4:1 methanol:ethanol). The remaining data are obtained from the analysis of resistivity measurements. The superconducting transition temperature, T_c , is multiplied by 4 for clarity.

1- or 2-D organic compounds [34, 35], and a number of elements at very high pressure [36]. There is an emerging view that in most cases the evolution of the phonon spectrum with tuning parameters like pressure crucially influences T_c , both by boosting it when the lattice instability is suppressed, and by reducing it again when pressure is increased further. Whereas most of the aforementioned materials are low-dimensional, very few clear cases of CDW order in 3D materials exist, notably cubic CuV_2S_4 [37], which is not superconducting, and orthorhombic $\alpha\text{-U}$ [38], for which a recent detailed examination of the phonon spectrum [39] suggests similarities to the mechanisms outlined above. $(\text{Sr}/\text{Ca})_3\text{Ir}_4\text{Sn}_{13}$ allows us to investigate the interaction between a structural instability and superconductivity in a cubic material. Our study clarifies the nature of the previously unidentified phase transition in $(\text{Sr}/\text{Ca})_3\text{Ir}_4\text{Sn}_{13}$, it demonstrates that this transition can be tuned to zero temperature, suggesting a structural quantum critical point, and it attributes the linear $\rho(T)$ and the dome structure of T_c to the associated softening of optical phonon modes. The prospect of fine-tuning phonon frequencies by controlling a structural transition temperature motivates further studies in this material class as well as in more complex systems, in which spin and charge density wave transitions may be correlated.

Acknowledgements We particularly thank G. G. Lonzarich, C. Pickard, and D. Khmel'nitskii for helpful discussions. This work was supported by the EP-SRC UK, Trinity College (Cambridge), Grant-in-Aid for Scientific Research from the JSPS (22350029), and the Global COE Program "International Center for Integrated Research and Advanced Education in Materials Science" at Kyoto University. SKG acknowledges the Great Britain Sasakawa Foundation for travel support and Kyoto University for hospitality.

* skg27@cam.ac.uk

† Current address: Department of Chemistry, University of Bath, Bath BA2 7AY, United Kingdom

- [1] I. Bersuker, *The Jahn-Teller Effect*, Cambridge University Press (2006).
- [2] P. A. Lee, T. M. Rice, and P. W. Anderson, *Phys. Rev. Lett.* **31**, 462 (1973).
- [3] J. Remeika, G. Espinosa, A. Cooper, H. Barz, J. Rowell, D. McWhan, J. Vandenberg, D. Moncton, Z. Fisk, L. Woolf, H. Hamaker, M. Maple, G. Shirane, and W. Thomlinson, *Solid State Communications* **34**, 923 (1980).
- [4] G. P. Espinosa, *Mater. Res. Bull.* **15**, 791 (1980).
- [5] H. Sato, T. Fukuhara, S. Iwakawa, Y. Aoki, I. Sakamoto, S. Takayanagi, and N. Wada, *Physica B* **186-88**, 630 (1993).
- [6] A. M. Strydom, *J. Phys.:Condens. Matter* **19**, 386205 (2007).
- [7] J. Hodeau, M. Marezio, J. Remeika, and C. Chen, *Solid State Communications* **42**, 97 (1982).
- [8] S. Miraglia, J. Hodeau, M. Marezio, C. Laviron, M. Ghedira, and G. Espinosa, *J. Solid State Chem.* **63**, 358 (1986).
- [9] P. Bordet, D. Cox, G. Espinosa, J. Hodeau, and M. Marezio, *Solid State Communications* **78**, 359 (1991).
- [10] J. Yang, B. Chen, C. Michioka, and K. Yoshimura, *J. Phys. Soc. Jpn.* **79**, 113705 (2010).
- [11] S. K. Goh, P. L. Alireza, P. D. A. Mann, A. M. Curnberlidge, C. Bergemann, M. Sutherland, and Y. Maeno, *Curr. Appl. Phys.* **8**, 304 (2008).
- [12] P. L. Alireza and S. R. Julian, *Rev. Sci. Instrum.* **74**, 4728 (2003).
- [13] L. E. Klintberg, S. K. Goh, S. Kasahara, Y. Nakai, K. Ishida, M. Sutherland, T. Shibauchi, Y. Matsuda, and T. Terashima, *J. Phys. Soc. Jpn.* **79**, 123706 (2010).
- [14] G. M. Sheldrick, *Acta Crystallographica Section A* **64**, 112 (2008).
- [15] L. J. Farrugia, *J. Appl. Cryst.* **32**, 837 (1999).
- [16] J. P. Perdew, K. Burke, and M. Ernzerhof, *Phys. Rev. Lett.* **77**, 3865 (1996).
- [17] K. Schwarz, and P. Blaha, *Computational Materials Science* **28**, 259 (2003).
- [18] See Supplemental Material at <http://link.aps.org/supplemental/...> for (i) crystal structure (.cif) as well as processed data (.hkl) files from single crystal x-ray diffraction on $\text{Sr}_3\text{Ir}_4\text{Sn}_{13}$, which provide information about relative intensity and associated errors of each observed reflection, (ii) the results of the Lindhard function calculation in $\text{Sr}_3\text{Ir}_4\text{Sn}_{13}$, (iii) further high pressure resistivity data of the $(\text{Sr}/\text{Ca})_3\text{Ir}_4\text{Sn}_{13}$ composition series.
- [19] M. D. Johannes, and I. I. Mazin, *Phys. Rev. B* **77**, 165135 (2008).
- [20] N. D. Mathur, F. M. Grosche, S. R. Julian, I. R. Walker, D. M. Freye, R. K. W. Haselwimmer, and G. G. Lonzarich, *Nature* **394**, 39 (1998).
- [21] N. Kase, H. Hayamizu, and J. Akimitsu, *Phys. Rev. B* **83**, 184509 (2011).
- [22] S. Y. Zhou, H. Zhang, X. C. Hong, B. Y. Pan, X. Qiu, W. N. Dong, X. L. Li, and S. Y. Li, arXiv:1202.5164 (2012).
- [23] J. R. Cooper, *Phys. Rev. B* **9**, 2778 (1974).
- [24] R. Lortz, Y. Wang, U. Tutsch, S. Abe, C. Meingast, P. Popovich, W. Knafo, N. Shitsevalova, Yu. B. Paderno, and A. Junod, *Phys. Rev. B* **73**, 024512 (2006).
- [25] W. L. McMillan, *Phys. Rev.* **167**, 331 (1968).
- [26] M. Calandra and F. Mauri, *Phys. Rev. Lett.* **106**, 196406 (2011).
- [27] L. Testardi, *Rev. Mod. Phys.* **47**, 637 (1975).
- [28] S. Tanaka, A. Miyake, B. Salce, D. Braithwaite, T. Kagayama, and K. Shimizu, *J. Phys.: Conf. Ser.* **200**, 012202 (2010).
- [29] R. Shelton, L. Hausermannberg, P. Klavins, H. Yang, M. Anderson, and C. Swenson, *Phys. Rev. B* **34**, 4590 (1986).
- [30] E. Morosan, H. W. Zandbergen, B. S. Dennis, J. W. G. Bos, Y. Onose, T. Klimczuk, A. P. Ramirez, N. P. Ong, and R. J. Cava, *Nature Physics* **2**, 544 (2006).
- [31] A. F. Kusmartseva, B. Sipos, H. Berger, L. Forro, and E. Tutis, *Phys. Rev. Lett.* **103**, 236401 (2009).
- [32] B. Sipos, A. Kusmartseva, A. Akrap, L. F. H. Berger, and E. Tutis, *Nature Materials* **7**, 960 (2008).
- [33] A. Gauzzi, S. Takashima, N. Takeshita, C. Terakura, H. Takagi, N. Emery, C. Herold, P. Lagrange, and G. Loupiaz, *Phys. Rev. Lett.* **98**, 067002 (2007).
- [34] W. Lubczynski, S. V. Demishev, J. Singleton, J. M. Caulfield, L. du Croo de Jongh, C. J. Kepert, S. J. Blundell, W. Hayes, M. Kurmoo, and P. Day, *J. Phys.: Condens. Matter* **8**, 6005 (1996).
- [35] J. Wosnitzer, *Curr. Opin. Solid State Mater. Sci.* **5**, 131 (2001).
- [36] O. Degtyareva, M. V. Magnitskaya, J. Kohanoff, G. Profeta, S. Scandolo, M. Hanfland, M. I. McMahan, E. Gregoryanz, *Phys. Rev. Lett.* **99**, 155505 (2007).
- [37] R. Fleming, F. DiSalvo, R. Cava, and J. Waszczak, *Phys. Rev. B* **24**, 2850 (1981).
- [38] G. H. Lander, E. S. Fisher, S. D. Bader, *Adv. Phys.* **43**, 1 (1994).
- [39] S. Raymond, J. Bouchet, G. Lander, M. L. Tacon, G. Garbarino, M. Hoesch, J.-P. Rueff, M. Krisch, J. Lashley, R. Schulze, and R. Albers, *Phys. Rev. Lett.* **107**, 136401 (2011).